Electronic Journal of University of Aden for Basic and Applied Sciences
EJUA-BA Vol. 4 No. 4 (2023)
https://doi.org/10.47372/ejua-ba.2023.4.296
ISSN: 2708-0684

RESEARCH ARTICLE

EVALUATION OF NUCLEAR RADIATION SHIELDING BEHAVIOR AND STRUCTURE PROPERTIES OF NOVEL B_2O_3-Na_2O-K_2O-xBi_2O_3 GLASSES

Dua'a Anis Taya[1], Adel A. M. Saeed[2] and Emran Eisa Saleh[1,*]

[1] *Physics department, Faculty of Science, University of Aden, Yemen P. O. 6312; edu-aa.anees.scie@aden-univ.net*
[2] *Chemistry department, Faculty of Science, University of Aden, Yemen P. O. 6312; adel_saeed73@yahoo.com*

***Corresponding author: Emran Eisa Saleh; E-mail: amran.isaa.scie@aden-univ.net; eesas2009@yahoo.com; Tel.: +201555049233; +967776413089**

Received: 29 August 2023 / Accepted: 11 September 2023 / Published online: 31 December 2023

Abstract

It was studied in this research the nuclear radiation shielding behavior and structure properties of the four glass samples which were composed of (80-x) B_2O_3-10Na_2O-10K_2O-xBi_2O_3 (x=0, 15, 30, 45 mol%) and were prepared using the melt-quenching technique. The studied samples were symbolized as Bi0.0, Bi0.15, Bi0.30, and Bi0.45 according to the Bi_2O_3 content values. The nuclear shielding properties have been calculated by the Phy-X/PSD program in the photon energy from 0.015 to 15 MeV. The results indicated that the values of mass attenuation coefficient (MAC) ranged from 4.2 to 88.5 cm^2/g, linear attenuation coefficient (LAC) values ranged from 8.99 to 429.99 cm^{-1}, half-value layer (HVL) values decreased from 0.077 to 0.002 cm, tenth value layer (TVL) values decreased from 1.570 to 0.020 cm, mean free path (MFP) values decreased from 0.682 to 0.009 cm, effective atomic number (Z_{eff}) values ranged from 12.9 to 77.5, effective electron density (N_{eff}) values ranged from 5.00 × 10^{23} to 8.60×10^{23} electrons/g, atomic and electron cross-sections (ACS and ECS) values ranged from 1.09 × 10^{-22} to 7.98 × 10^{-21} cm^2/g and from 8.47 × 10^{-24} to 1.03 × 10^{-22} cm^2/g respectively. The effective neutron removal cross-section (Σ_R) values for prepared samples were also calculated. The results indicated that the addition of bismuth oxide leads to an improvement in the nuclear shielding properties of the prepared glass and showed that the sample Bi0.45 has the best nuclear shielding properties than concrete and commercial glasses.

Keywords: Nuclear shielding, Nuclear parameters, Glasses, Gamma rays, Bi_2O_3

1. Introduction

There is a growing use of ionizing radiation in various fields such as medical physics, imaging and radiotherapy, nuclear reactors, and space technology applications. [1]. Therefore, it is very important to develop the best radiation protection materials. It is possible to use any compound as protection from nuclear radiation if the thickness of this material is sufficient to absorb radiation to reach a safe state [2]. The researchers were interested in developing protective materials according to the type of radiation and the method of application. Some materials have high atomic numbers that make them suitable for protection from X-rays, gamma rays, and neutrons such as concrete, lead, and their counterparts [3]. These materials are widely used in the protection of high-energy rays and have many advantages, but they have some disadvantages such as opacity, humidity levels lead to a change in the shielding properties of concrete, cracks occur in concrete shields and water loss due to prolonged exposure to radiation, in addition to the toxic effects of lead on the environment [4].

Concern about lead toxicity has increased in the past few years, as the effect of lead toxicity in children and adults has been studied [5,6]. Environmentally friendly, non-toxic "lead-free" shielding has become a challenging requirement. Currently, in many radiation protection applications lead oxide glasses have been restricted [7]. The glass industry has developed rapidly in recent years due to the low cost of raw materials used in its manufacture as well as the simplicity of the way it is prepared [8]. It is also transparent, and its properties are easy to modify by changing its chemical composition [9], since its ability to protect against gamma rays can be improved by adding some oxides in certain proportions to be used as a gamma ray shield [10].

The current study aims to manufacture a new type of lead-free glass using melt-quenching technique and evaluate its

effectiveness in protecting against gamma rays by investigating the nuclear shielding parameters using the Phy-x program [11].

2. Materials and Methods

2.1. Sample Preparation and Characterization Techniques

A borate glass was synthesized and doped with some oxides of elements and prepared by the melt-quenching technique. After mixing and grinding materials, mixed quantities were placed in porcelain crucibles and inserted into an electric furnace for melting and held at 1000 ºC for 0.5 hour. The samples were poured on a molding mold, and then immediately transferred to an annealing furnace held at 250 °C, for 1.5 hours, then the furnace was switched off to allow the glass to cool gradually to room temperature. The glass samples were kept in the dried furnace for one day to prevent moisture entry into the samples.

The XRD spectrum was obtained by an XRD device to explore the nature of the samples. The density of the prepared samples was also calculated using Archimedes method.

2.2. Melt Quenching Method

The melt quenching method is the oldest and one of the most popular and established methods for preparing glass. When the mixture of chemicals in this process is cooled down rapidly, an amorphous material (which exhibits glass-transition phenomenon are often designated as “glasses”) is formed from the molten phase. The distinguishing feature of the melt-quenching process is that the amorphous solid is formed by the “continuous” hardening (i.e., increase in viscosity) of the melt. The essential condition for “glass” formation from the melt is that the cooling is sufficiently fast to avoid crystal nucleation and growth. The essential condition for glass formation, lies in the nucleation rate, should be less than a certain value (10^{-6} $cm^{-1}s^{-1}$). Crystallization of the melt occurs as a discontinuous solidification at the liquid-solid interface where solid growth takes place only, with the result that crystallites grow in the body of the melt. The crystal growth will always dominate over the formation of the amorphous phase [17].

2.3. Archimedes' Principle

The Archimedes’ principle, a physical law of buoyancy, was discovered by the ancient Greek mathematician and inventor Archimedes, stating that anybody completely or partially submerged in a fluid (gas or liquid) at rest is acted upon by an upward, or buoyant, force, the magnitude of which is equal to the weight of the fluid displaced by the body. The density of the prepared samples was measured using the Archimedes' principle. The samples were measured firstly at room temperature (25 ºC) in the air and then in the buoyant liquid (toluene) using the sensitive balance with a sensitivity of (±0.0001g). The density of the prepared samples was calculated using the following equation:

$$\rho=A/(A-B)\times\rho_0 \qquad (1)$$

where A is the weight of the sample in air, B is the weight of sample in toluene and ρ_0 is the density of toluene (0.87 g/cm^3).

2.4. Computational Work

A user-friendly online Photon Shielding and Dosimetry (PSD) software available at https://phy-x.net/PSD is utilized for the calculation of nuclear radiation shielding parameters.

2.4.1. Linear Attenuation Coefficient (LAC)

The LAC is defined as the interaction probability of a photon per unit distance of the medium it traverses. When a collimated beam of monochromatic photons with an intensity of I_0 impinges on a material of thickness x, a portion of the beam photons interacts with the material and this causes a decrease in the initial intensity (I_0). The transmitted intensity is labelled I, the total linear attenuation is given by the following formula [12]:

$$\mu = \frac{1}{x} ln \frac{I_0}{I} \qquad (2)$$

2.4.2. Mass Attenuation Coefficient (MAC)

The MAC is the linear attenuation coefficient per unit mass of the materials. One of the most important factors of material in absorbing and scattering radiation is MAC. The total mass attenuation coefficients are given by the equation below [12, 13]:

$$\text{MAC} = \frac{\mu}{\rho} = \frac{1}{\rho x} ln \frac{I_0}{I} \qquad (3)$$

x and ρ are the thickness and density of the materials, respectively.

2.4.3. The Half Value Layer (HVL)

The HVL is the thickness of any given material, at which 50% of the incident energy has been attenuated. It is given by [14]:

$$\text{HVL}= \frac{ln\,2}{\mu} \qquad (4)$$

2.4.4. Tenth Value Layer (TVL)

The TVL is the thickness of any given material, at which 10% of the incident energy has been attenuated. It is given by [14]:

$$\text{TVL}=\frac{ln\,10}{\mu} \qquad (5)$$

2.4.5. Mean Free Path (MFP)

The mean free path represents the average distance that a photon can travel between successive interactions [12]. In other words, the mean free path (MFP) is the average distance a nuclear radiation photon can travel in the prepared glass before being interacted. It is given by [15]:

$$MFP=\frac{1}{\mu} \quad (6)$$

2.4.6. Effective Atomic Number (Zeff)

For a medium consisting of different elements, the effective atomic number is calculated from the atomic numbers of the constituent elements, weighted according to the different partial photon interaction processes for composite material [12,13]. It is given by:

$$Z_{eff}=\frac{\sum_i f_i A_i \left(\frac{\mu}{\rho}\right)_i}{\sum_j \frac{A_j}{z_j}\left(\frac{\mu}{\rho}\right)_j} \quad (7)$$

where (μ/ρ) is the mass attenuation coefficient, μ is the linear attenuation coefficient, f_i, A_i, Z_i are a molar fraction, atomic mass, and atomic number, respectively.

2.4.7. Effective Electron Density (Neff)

It is expressed in number of electrons per unit mass. For a chemical element, the electron density is given by N_{eff} = NAZ/A. This expression can be generalized to compound [16]:

$$N_{eff}=N_A\frac{nz_{eff}}{\Sigma_i n_i A_i}=N_A\frac{z_{eff}}{\langle A\rangle} \quad (8)$$

where ⟨A⟩ is the average atomic mass of the compound.

N_{eff} can be determined using MAC and ECS values with the help of the following practical formula [18]:

$$N_{eff}=\frac{MAC}{ECS} \quad (9)$$

2.4.8. Atomic and Electron Cross-Sections (ACS and ECS)

The ACS wouldn't be an actual area of the atom, but would be an effective area for an interaction between the photon and the atom that is being considered. The total atomic cross-section for compound materials can be obtained using the following relationship [13,19]:

$$ACS=\sigma_t=\frac{\mu_m N}{N_A} \quad (10)$$

where μ_m is the atomic attenuation coefficient, N=Σ niAi is the atomic mass of materials, and N_A is Avogadro's number.

The total electronic cross section (ECS) of the materials can be found by the following relationship [13]:

$$ECS=\sigma_e=\frac{\sigma_t}{z_{eff}} \quad (11)$$

2.4.9. Effective Fast Neutron Removal Cross-Section (FNRCS) (∑R)

It is the probability that a fast or fission energy neutron undergoes a first collision, which removes it from the group of penetrating, uncollided neutrons. the effective removal cross-section for fast neutrons, $\sum_R$ can be calculated for mixtures, alloys, and compounds by the equation:

$$\Sigma_R=\Sigma_i w_i(\Sigma_R)_i \quad (12)$$

where w_i is the weight percentage, and $\sum_R$ is the effective removal cross-section for fast neutrons of the constituting elements. $\sum_R$ can be determined as a function of the atomic weight A and the atomic number Z by the following empirical formulas [20]:

$$\Sigma_R=0.21\,A^{-0.56}\ cm^2g^{-1} \quad (13)$$

$$\Sigma_R=0.00662A^{-1/3}+0.33\,A^{-2/3}-0.211A^{-1}\ cm^2g^{-1}(A>12) \quad (14)$$

$$\Sigma_R=0.190\,Z^{-0.743}\ cm^2g^{-1}\ (Z\le 8) \quad (15)$$

$$\Sigma_R=0.125\,Z^{-0.565}\ cm^2g^{-1}\ (Z>8) \quad (16)$$

3. Results and Discussion

3.1 The Densities and Structural Properties of the Prepared Glass Samples

The density of the prepared glass samples was plotted in Table (1). The samples' density has increased from 2.1 g/cm^3 to 4.9 g/cm^3 with increasing Bi_2O_3 content, because of the high molecular weight of bismuth oxide (465.96 g/mol). The XRD pattern of the series is shown in Fig. (1). It is clear that there are smooth peaks in the spectra of the samples, which explains the amorphous of the prepared samples.

Table 1. The densities of the glass samples

Sample	Density (g/cm^3)	AMW (g/mol)
Bi 0.0	2.1	71.3
Bi 0.15	3.6	130.8
Bi 0.30	4.7	190.2
Bi 0.45	4.9	249.7

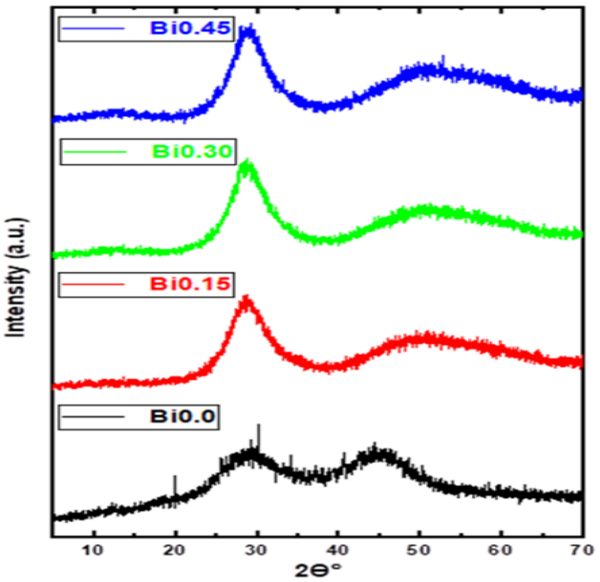

Figure 1. The XRD pattern of the series

3.2. The Nuclear Radiation Shielding Properties of the Prepared Samples

All parameters of prepared samples were estimated by Phy-X/PSD software program [11].

3.2.1. The Mass Attenuation Coefficient (MAC) of the Samples

Figure 2. demonstrates the values of MAC of all prepared glass samples for the energy range from 0.015 to 15 MeV. The highest values of MAC were 4.2, 57.9, 78.0, and 88.5 cm^2/g at the energy 0.015 MeV for Bi0.0, Bi0.15, Bi0.30, and Bi0.45 respectively. The lowest value of MAC is Bi0.0, and the sample Bi0.45 possesses the highest value of the MAC among the other prepared samples because it has the highest density than other.

The MAC decreases rapidly for all samples in the low energy photon as shown in Fig. (2). In this region the photoelectric effect is dominant, and its cross-section is proportional to $Z^5/E^{3.5}$, then the MAC values increase suddenly at 90.5 keV which is the value of absorption K-edge for bismuth. After that, the MAC values decrease slowly until they reach the minimum values, in this region the Compton effect is dominant, which its cross-section is proportional to Z/E. Finally, the MAC values increase again due to pair production interaction and, in this region, the pair production is dominant, which its cross section is proportional to Z^2 and logarithm E of the energy of incident photon.

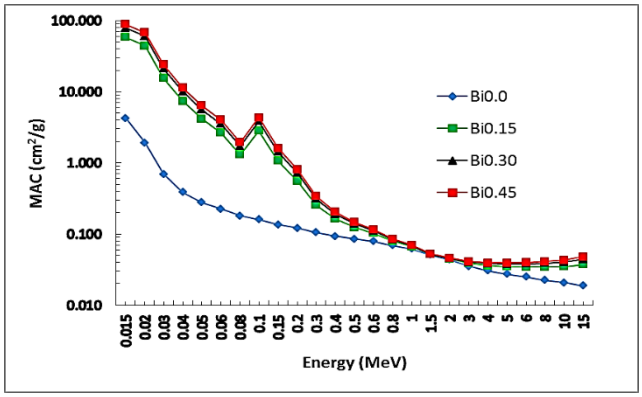

Figure 2. Mass attenuation coefficient values of the prepared samples

3.2.2 The Linear Attenuation Coefficient (LAC) of the Samples

The LAC values versus the photon energy of the prepared samples are shown in Fig. (3). The highest values of LAC are 8.99, 210.5, 370.4, and 429.9 cm^{-1} at the energy 0.015 MeV for Bi0.0, Bi0.15, Bi0.30, and Bi0.45, respectively. Bi0.0 sample has the lowest value of LAC, and the Bi0.45 sample possesses the highest value of the LAC among the other prepared samples because the LAC increases with increasing the density, where there is the direct relationship between LAC and density. The behavior of the LAC is similar to the behavior of the MAC.

3.2.3. The Half Value Layer (HVL)

The values of the HVL versus the energy of the photon of the prepared glass samples are shown in Fig. (4). The lowest values of HVL were 0.077, 0.003, 0.002, and 0.002 cm at energy 15 KeV for Bi0.0, Bi0.15, Bi0.30, and Bi0.45, respectively. In this reign, the photoelectric effect is dominant. It is clear that the values of HVL decrease with increasing the density of samples (due to excess bismuth content). The sample Bi0.45 has the lowest values of HVL, so it has higher radiation absorption efficiency.

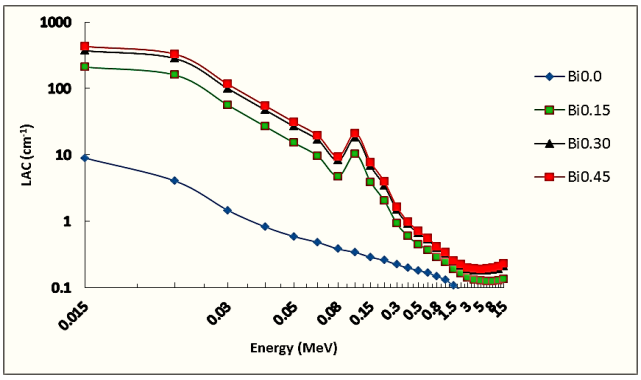

Figure 3. Linear attenuation coefficient values of the series samples

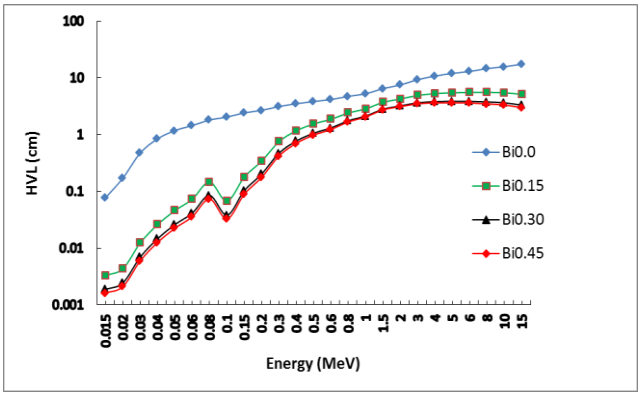

Figure 4. Half-value layer values of the glass samples

3.2.4 The Tenth Value Layer (TVL) of the Samples

From Fig. (5) the lowest values of TVL in the series samples were 0.256, 0.011, 0.006, and 0.005 cm at energy 15 KeV for Bi0.0, Bi0.15, Bi0.30, and Bi0.45 respectively. The sample Bi0.45 has the lowest value of TVL because it has the highest density, so it has higher radiation absorption efficiency. The TVL values decrease with increased densities of the samples. The behavior of the TVL is similar to the behavior of the HVL which was explained before.

3.2.5 The Mean Free Path (MFP) of the Glass Samples

The MFP is inversely relation with LAC, so the MFP decreases when the density of the samples increases, and it increases when the photon energy increases as shown in Fig. (6). The lowest values of MFP in the prepared glass

samples were 0.111, 0.005, 0.003, and 0.002 cm at energy 15 KeV for Bi0.0, Bi0.15, Bi0.30, and Bi0.45 respectively. The behavior of the MFP is similar to the behavior of the TVL and HVL. The sample Bi0.45 has the lowest value of MFP because it has the highest linear attenuation coefficients LAC.

3.2.6 The Effective Atomic Number (Zeff)

The Z_{eff} is linked with MAC. The Z_{eff} versus the photon energy of the prepared glass samples is shown in Fig. (7). The highest values of Z_{eff} were 12.9, 73.4, 77.94, and 79.64 at the energy 16.38 KeV for Bi0.15, Bi0.30, and Bi0.45 respectively, due to the absorption L-edge of bismuth. Sample Bi0.0 has the lowest value of Z_{eff}, and the Bi0.45 sample possesses the highest value of the Z_{eff} among the other prepared samples because it has the highest density than other due to the highest bismuth element content.

The Z_{eff} decreases for all samples with increasing photon energy. In this region the photoelectric effect is dominant, which its cross section is proportional to $Z^5/E^{3.5}$, then the Z_{eff} value increases suddenly at 90.5 keV which is the value of absorption k-edge for bismuth. After that, the Z_{eff} decreases slowly until it reaches the minimum values, in this region the Compton effect is dominant, and its cross-section is proportional to Z/E. Finally, the Z_{eff} values increase again due to pair production interaction, in this region, the pair production is dominant, which its cross section is proportional to Z^2 and logarithm E of the energy of an incident photon.

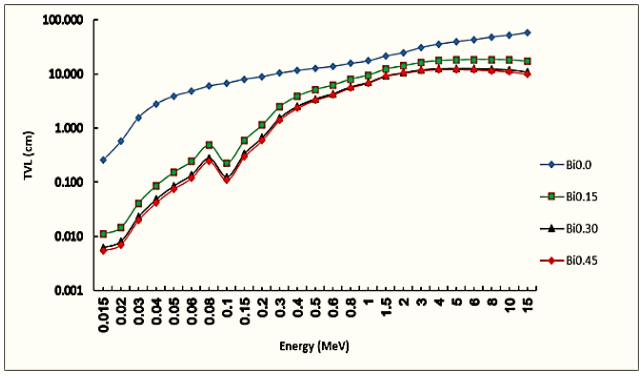

Figure 5. Tenth value layer values of the series samples

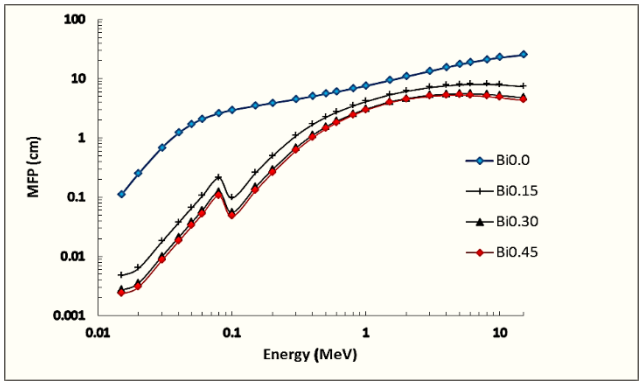

Figure 6. Mean free path values of the series samples

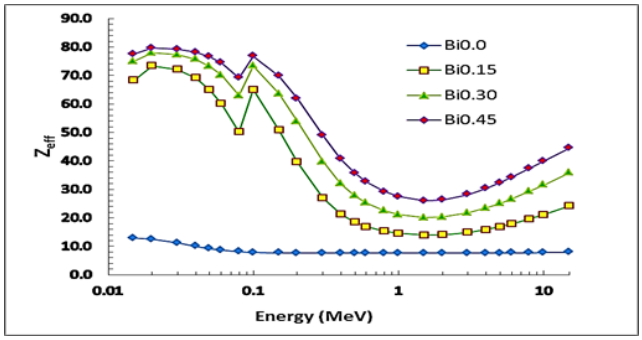

Figure 7. Effective atomic numbers of the prepared glass samples

3.2.7 The Effective Electron Density (Neff)

The N_{eff} versus the photon energy of the series samples is shown in Fig. (8). The highest values of N_{eff} are 5.00×10^{23} electrons/g at 0.015 MeV for Bi0.0 sample and 1.55×10^{24}, 1.14×10^{24}, and 8.83×10^{23} electrons/g at the energy 16.38 KeV for Bi0.15, Bi0.30, Bi0.45 respectively, which is the value of absorption L-edge of bismuth. The N_{eff} is decreasing with increasing the bismuth content due to increased ECS. The behavior of N_{eff} is similar to the behavior of Z_{eff}.

3.2.8 The Atomic Cross Section (ACS) of the Prepared Glass Samples

Figure (9) demonstrates the values of ACS of all prepared glass samples, for the energy range from 0.015 to 15 MeV. The highest values of ACS were 1.09×10^{-22}, 2.73×10^{-21}, 5.36×10^{-21}, 7.98×10^{-21} cm^2/g at the energy 0.015 MeV for Bi0.0, Bi0.15, Bi0.30, and Bi0.45, respectively. The Bi0.45 sample possesses the highest value of the ACS among the other prepared samples because it has the highest density due to its highest bismuth content, and the lowest value of ACS is for Bi0.0. The ACS values decrease rapidly for all samples with increasing photon energy. In this region the photoelectric effect is dominant, and its cross-section is proportional to $Z^5/E^{3.5}$, then the ACS values increase suddenly at 90.5 keV which is the value of the absorption K-edge for bismuth. After that, the ACS values decrease slowly until they reach the minimum values, in this region the Compton effect is dominant, which its cross-section is proportional to Z/E. Lastly, the ACS increases again due to pair production interaction, in this region, the pair production is dominant, which its cross section is proportional to Z^2 and logarithm E of the energy of an incident photon.

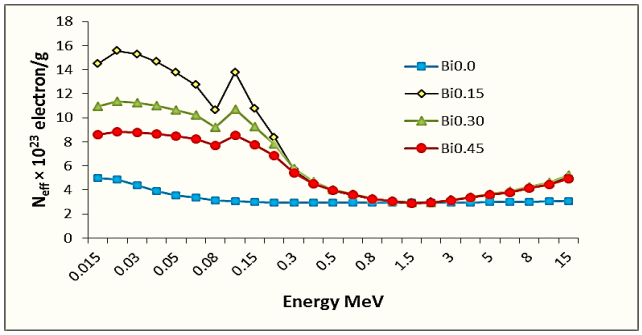

Figure 8. Effective electron density of series samples

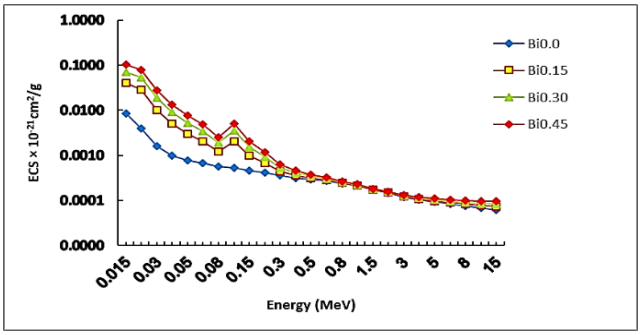

Figure 10. Electron cross-section of the series samples

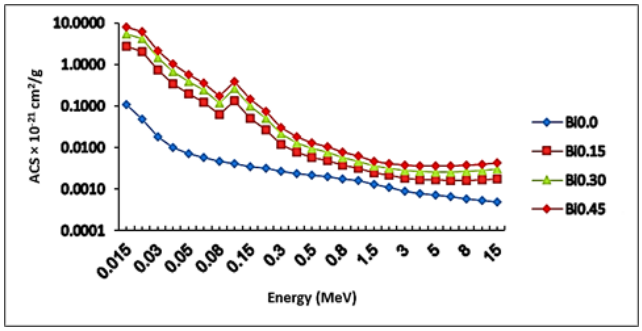

Figure 9. Atomic cross-section of the series samples

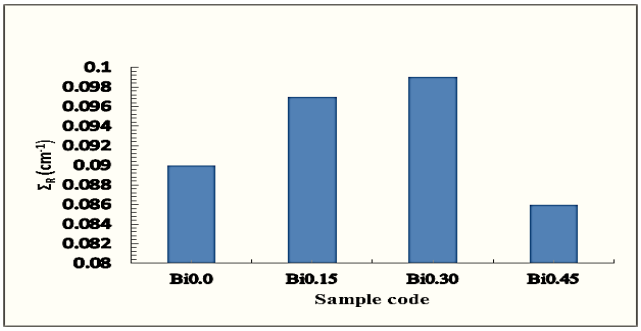

Figure 11. Fast neutron removal cross-section of the series samples

3.2.9 The Electron Cross Section (ECS) of the Prepared Samples

The ECS versus the photon energy of the prepared glass samples is shown in Fig. (10). The highest values of ECS are 8.47×10^{-24}, 4.00×10^{-23}, 7.15×10^{-23}, and 1.03×10^{-22} cm^2/g at the energy 0.015 MeV for Bi0.0, Bi0.15, Bi0.30, and Bi0.45 respectively. The lowest value of ECS is for Bi0.0 sample, and the sample Bi0.45 possesses the highest value of the ECS among the other prepared glass samples because the ECS is increasing with increasing the density due to increased bismuth content. The behavior of the ECS is similar to the behavior of the ACS.

3.2.10 The Fast Neutron Removal Cross Section (FNRCS) of the samples

The fast neutron removal cross sections (FNRCS) values of the samples are shown in Fig. (11). The values were 0.090, 0.097, 0.099, and 0.086 cm^{-1} for Bi0.0, Bi0.15, Bi0.30 and Bi0.45 samples, respectively. The best value of FNRCS is 0.099 cm^{-1} which is for the sample Bi0.45, and the lowest value of FNRCS is 0.086 cm^{-1} for Bi0.0 sample, which has the highest average molecular weight (AMW) and density due to the high content of bismuth element.

3.3 Comparing the Results with the Concrete and Commercial Glasses

3.3.1 Comparison Between MAC for Bi0.45 Glass Sample with Concrete and Commercial Glasses

It can be noticed in Fig. (12) that the presented sample Bi0.45 has the highest MAC values than commercial glasses (Pb40, Cr, Rs 253 G18, and Rs-360) and OC concrete (ordinary concrete), except BaC concrete (barite concrete) in the energy range 0.04-0.08 MeV.

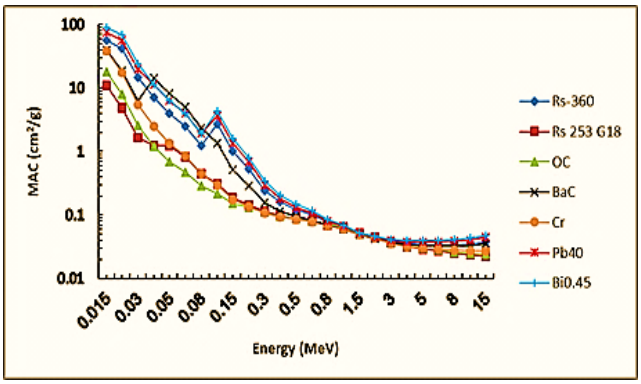

Figure 12. Comparison between MAC for Bi0.45 sample with concrete and commercial glasses

3.3.2 Comparison Between HVL for Bi0.45 Sample with Concrete and Commercial Glasses

Figure (13) demonstrates that the HVL of Bi0.45 and Pb40 is convergent and lower than the values of the other concrete and commercial glasses.

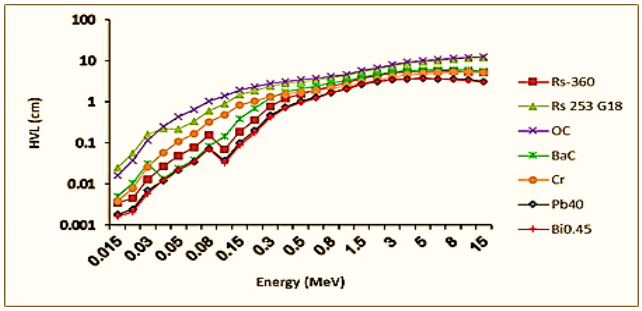

Figure 13. Comparison between HVL for Bi0.45 sample with concrete and commercial glasses

3.3.3 Comparison Between Zeff for Bi0.45 Sample with Concrete and Commercial Glasses

The results represented in Fig. (14) indicate that the Z_{eff} for the presented sample Bi0.45 gave the highest and best results compared to the concrete (OC and BaC) and commercial glasses (Pb40, Cr, Rs 253 G18, and Rs-360).

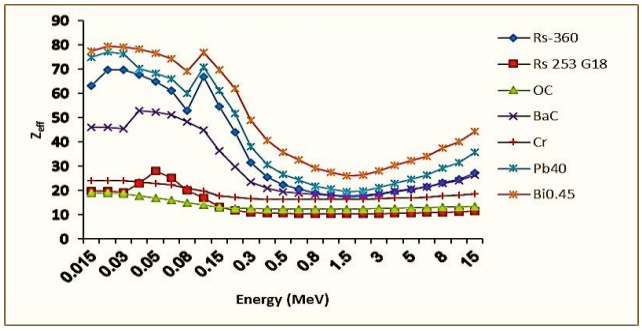

Figure 14. Comparison between Z_{eff} for Bi0.45 sample with concrete and commercial glasses

4. Conclusions

Due to the increased use of nuclear radiation in various fields, which has become important to improve radiation protective materials. The studies have proven that the toxic effects of many types of nuclear radiation protective glass because it contains lead or lead oxide also there are some shortcomings in common concrete. This research aims to prepare environmentally friendly glass samples and effective in protecting against gamma rays and fast neutrons. These samples were doped with heavy metal oxides (bismuth oxide) to be a radiation protective alternative by using a melt quenching technique, and the series samples was composed of $(80\text{-}x)B_2O_3 + 10Na_2CO_3 + 10K_2CO_3 + xBi_2O_3$ where x = 0, 15, 30, and 45. According to the results the XRD pattern indicated that all samples were amorphous, and the increasing bismuth oxide content lead to increase in the densities of the samples, MAC, LAC, Z_{eff}, ACS, ECS values and decreasing HVL, TVL, MEP, N_{eff} values. The results showed that the Bi0.45 sample has the best prepared samples for protection nuclear radiation. And from compared our prepared samples with the concrete (OC and BaC) and commercial glasses (Pb40, Cr, Rs 253 G18, and Rs-360) the results showed that our prepared samples have the best nuclear radiation protection properties.

Author Contributions:

Conceptualization, E.E Saleh, A.A. Saeed; methodology, E. E. Saleh; software, E. E. Saleh, D. A. Taya; validation, E. E. Saleh, A. A. Saeed; formal analysis, E. E. Saleh, D. A. Taya; investigation, D. A. Taya and E. E. Saleh; resources, E. E. Saleh, D. A. Taya; data curation, E. E. Saleh, A.A. Saeed; writing original draft preparation, D. A. Taya; writing review and editing, E. E. Saleh, A. A. Saeed; visualization, E. E. Saleh, A. A. Saeed ; supervision, E. E. Saleh, A. A. Saeed; project administration, E. E. Saleh, D. A. Taya; funding acquisition, D. A. Taya. All authors have read and agreed to the published version of the manuscript.

Funding:

This research received no external funding.

Acknowledgments:

The authors extend their appreciation to the Employees of the Yemeni Geological Authority, Aden, Ministry of Oil and Minerals, Yemen for technical support.

Conflicts of Interest:

The authors declare no conflict of interest.

References

[1] M. Kurudirek, "Heavy metal borate glasses: Potential use for radiation shielding", J. Alloy Compd. 2017, vol. 727, pp.1227-1236 doi: https://doi.org/10.1016/j.jallcom.2017.08.237

[2] S.A.M. Issa; Y.B. Saddeek; H.O. Tekin; M.I. Sayyed; K.S. Shaaban, "Investigations of radiation shielding and elastic properties of PbO-SiO2-B2O3-Na2O glasses using Monte Carlo method", Curr. Appl. Phys, 2008, vol. 18, no. 6, pp.717-727, doi: https://doi.org/10.1016/j.cap.2018.02.018

[3] A. El-Taher; A.M. Ali; Y.B. Saddeek; R. Elsaman; H. Algarni; K. Shaaban; T.Z. Amer, "Gamma ray shielding and structural properties of iron alkali alumino-phosphate glasses modified by PbO", Radiat. Phys. Chem. 2019, vol. 165, 108403. doi: https://doi.org/10.1016/j.radphyschem.2019.108403

[4] A.A.A. Darwish; S.A.M. Issa; M.M. El-Nahass, "Effect of gamma irradiation on structural, electrical and optical properties of nanostructure thin films of nickel phthalocyanine", Synth. Met. 2016, vol. 215, app. 200–206. doi: https://doi.org/j.synthmet.2016.03.002/10.1016

[5] E. E. Saleh; M. A. Algradee; F. Alresheedi; M. S.Al-Fakeh; S. A. El-Fiki; G.M. Youssef; T. El Sharbini, "Synthesis and nuclear radiation shielding ability of Li_2O-ZnO-P_2O_5 glasses: The role of Yb_2O_3", J. Electron. Mater. vol. 51, pp. 7283–7296. doi: https://doi.org/10.1007/s11664-022-09979-9

[6] E. Millstone; J. Russell, "Lead toxicity and public health policy", J. R. Soc. Health.1995, vol. 115, pp. 347–350. doi: https://doi.org/10.1177/146642409511500603 . PMID: 8568780

[7] S.Vishwanath; N.M. Badiger; J. Kaewkhao, "Radiation shielding competence of silicate and borate heavy metal oxide glasses: comparative study", J. Non-Cryst. Solids. 2014, vol 404, pp. 167-173. doi: https://doi.org/10.1016/j.jnoncrysol.2014.08.003

[8] M.S. Al-Buriahi; B.T.Tonguc ,"Mass attenuation coefficients, effective atomic numbers and electron densities of some contrast agents for computed tomography", Radia. Phys. Chem. 2020, vol. 166. doi: https://doi.org/10.1016/j.radphyschem.2019.108507

[9] S.A.M. Issa; H.O. Tekin; T.T. Erguzel; G. Susoy, "The effective contribution of PbO on nuclear shielding properties of xPbO-(100−x) P_2O_5 glass system: a broad range investigation", Appl. Phys. A. 2019, vol. 125, 640. doi: https://doi.org/10.1007/s00339-019-2941-x

[10] A.A. Rammah; Y.M. Shaaban, "The influence of TiO_2 on structural, physical and optical properties of B_2O_3 – TeO_2 – Na_2O – CaO glasses", J. Non-Cryst. Solids. 2019, vol. 514, pp. 52–59. doi: https://doi.org/10.1016/j.jnoncrysol.2019.03.030

[11] E. Şakar; Ö.F. Özpolat; B. Alım; M.I. Sayyed; M. Kurudirek, "Phy-X/PSD: Development of a user friendly online software for calculation of parameters relevant to radiation shielding and dosimetry", Radiat. Phys. Chem. 2019, vol. 166, 108496. doi: https://doi.org/10.1016/j.radphyschem.2019.108496

[12] I. Akkurt; B. Mavi; A. Akkurt; C. Basyigit; S. Kilincarslan; H.A. Yalim, "Study on Z dependence of partial and total mass attenuation coefficients", JQSRT. 2004, 09, 024. doi: https://doi.org/10.1016/j.jqsrt.2004.09.024

[13] E.E.Saleh; M.A. Algradee; M. S. Al-Fakeh, "Nuclear radiation shielding behavior for prepared LNZP glasses doped with (CdO+Te)," Radia. Phys. Chem. 2021, vol.189, 109743. doi: https://doi.org/10.1016/j.radphyschem.2021.109743

[14] A. Akkas, "Determination of the tenth and half value layer thickness of concretes with differentd densities," Acta Phys. Pol. 2016, vol.129, no. 4, pp. 770-772. doi: https://doi.org/10.12693/APhysPolA.129.770

[15] P. Kaur; D. Singh; T. Singh, "Heavy metal oxide glasses as gamma rays shielding material", Nucl. Eng. Des. 2016, vol. 307, pp.364-376. doi: https://doi.org/10.1016/j.nucengdes.2016.07.029

[16] S.R. Manohara; S. M. Hanagodimath; K.S.Thind; L. Gerward, "On the effective atomic number and electron density: a comprehensive set of formulas for all types of materials and energies above 1 keV," Nucl. Instrum. Methods. Phys. 2008, vol266, no. 18, pp. 3906-3912. doi: https://doi.org/10.1016/j.nimb.2008.06.034

[17] S. Bhattacharya, "Metal oxide glass nanocomposites". 2020, Elsevier Press.

[18] M. A. Algradee; E. E. Saleh; O. M. Samir; A. B. Alwany; T. M. EL Sherbini, "Evaluation of structural, elastic properties and nuclear radiation shielding competence of Nd^{3+} doped lithium-zinc-phosphate glasses", J. Non Cryst. Solids. 2022, vol. 576,121304. doi: https://doi.org/10.1016/j.jnoncrysol.2021.12130 4

[19] E. E. Saleh; M. A. Algradee; S. A. El-Fiki; G. M. Youssef, "Fabrication of novel lithium lead bismuth borate glasses for nuclear radiation shielding," Radia. Phy. chem. 2022, vol. 193,1009939. doi: https://doi.org/10.1016/j.radphyschem.2021.109939

[20] M. A. Algradee; E. E. Saleh; T. M. El Sherbini; R. El-Mallawany, "Optical and gamma-ray shielding features of Nd^{3+} doped lithium-zinc-borophosphorate glasses", Optik. 2021, vol. 242, 167059. doi: https://doi.org/10.1016/j.ijleo.2021.167059

مقالة بحثية

تقييم سلوك الحجب من الإشعاع النووي وخصائص هيكل زجاجات B_2O_3-Na_2O-K_2O-xBi_2O_3 الجديدة

دعاء أنيس طايع[1]، عادل أحمد سعيد[2]، عمران عيسى صالح[1،*]

[1] قسم الفيزياء، كلية العلوم، جامعة عدن، اليمن؛ edu-aa.anees.scie@aden-univ.net
[2] قسم الكيمياء، كلية العلوم، جامعة عدن، اليمن؛ adel_saeed73@yahoo.com

* الباحث الممثّل: عمران عيسى صالح؛ البريد الالكتروني: amran.isaa.scie@aden-univ.net; eesas2009@yahoo.com ؛+967776413089

استلم في: 29 أغسطس 2023 / قبل في: 11 سبتمبر 2023 / نشر في 31 ديسمبر 2023

المُلخّص

في هذا البحث تم تحضير عينات زجاجية مكونة منB_2O_3-10Na_2O-10K_2O-xBi_2O_3 (80-x)، (x = 0،15، 30، 45 مول%) باستخدام تقنية الصهر والتبريد. تم ترميز العينات المدروسة بـ Bi0.0، Bi0.15، Bi0.30، وBi0.45 طبقاً لقيم محتوى Bi_2O_3. تم حساب خصائص الحجب من الإشعاع بواسطة برنامج Phy-X/PSD في طاقة الفوتون من 0.015 إلى 15 MeV. أشارت النتائج إلى أن قيم معامل التوهين الكتلي (MAC) تراوحت من 4.2 إلى 88.5 سم^2/جم، وتراوحت قيم معامل التوهين الخطي (LAC) من 8.99 إلى 429.99 سم$^{-1}$، وانخفضت قيم طبقة نصف القيمة (HVL) من 0.077 إلى 0.002 سم، انخفضت قيم طبقة القيمة العاشرة (TVL) من 1.570 إلى 0.020 سم، وانخفض متوسط قيم المسار الحر (MFP) من 0.682 إلى 0.009 سم، وتراوحت قيم العدد الذري الفعال (Z_{eff}) من 12.9 إلى 77.5، وتراوحت قيم كثافة الإلكترونات الفعالة (N_{eff}) من 5.00 × 10^{23+} إلى 8.60×10^{23+} إلكترون/جم، بينما تراوحت قيم المقاطع العرضية الذرية والإلكترونية (ACS وECS) من 1.09 × 10^{-22} إلى 7.98 × 10^{-21} سم^2/جم ومن 8.47 × 10^{-24} إلى 1.03 × 10^{-22} سم^2/جم على التوالي. تم أيضًا حساب قيم المقطع العرضي الفعال لإزالة النيوترونات (Σ_R) للعينات المحضرة. أشارت النتائج إلى أن إضافة أكسيد البزموت أدى إلى تحسين خصائص الحجب النووي للزجاج المحضر، كما أظهرت أن العينة Bi0.45 تمتلك خصائص حجب نووي أفضل من الخرسانة والزجاج التجاري.

الكلمات المفتاحية: الحجب النووي، المعلمات النووية، الزجاج، أشعة جاما، Bi_2O_3.

How to cite this article:

D. A. Taya, A. A. Saeed, E. E. Saleh, "EVALUATION OF NUCLEAR RADIATION SHIELDING BEHAVIOR AND STRUCTURE PROPERTIES OF NOVEL B_2O_3-Na_2O-K_2O- xBi_2O_3 GLASSES", *Electron. J. Univ. Aden Basic Appl. Sci.*, vol. 4, no. 4, pp. 305-313, December. 2023. DOI: https://doi.org/10.47372/ejua-ba.2023.4.296